



Study of long-term performance and radiation damage of the SCT using conditions data

Jonas Rembser, Swiss Federal Institute of Technology in Zurich

September 16, 2015

Abstract

The long-term evolution of the SCT noise occupancy, efficiency and noisy strip count is presented. The SCT performance is stable over time, except a steady degradation due to radiation damage. Furthermore, the noise occupancy is checked for modulations that could hint to an origin in radiation damage: dependence on the distance to the interaction point, correlation between different parts of the detector and recovery during LHC downtime. Finally, the noise occupancy of individual modules is investigated. We find unpredictable increases, which recover slowly and steady, hinting they are not only statistical fluctuations, but an explanation has not been established.

Contents

1	Introduction	3
2	SCT calibration and conditions data	5
2.1	Calibration between LHC fills	5
2.2	Prompt calibration loop	5
2.3	Conditions data used in this work	6
2.4	Radiation damage and conditions data	7
3	Results and analysis	8
3.1	Time evolution of the number of noisy strips	8
3.2	Time evolution of the noise occupancy	9
3.3	Time evolution of the efficiency	10
3.4	Correlation and distance dependence of the noise occupancy	12
3.5	Analyzing individual modules	13
4	Conclusion	16

1 Introduction

The ATLAS [3] detector is one of the two multipurpose detectors at LHC, the other one being the CMS detector. It is made up of several subdetectors arranged around the interaction point (IP). Closest to the IP is the Inner Detector (ID), which is surrounded by the calorimeters and the muon chambers and is responsible for tracking charged particles. It can be seen in Figure 1. The ID itself consists of three subdetectors. In the center is the Pixel Detector, which is based on semiconductor technology. The outermost one is a gas detector, called the Transition Radiation Tracker (TRT). In between is the Semiconductor Tracker (SCT), a silicon microstrip detector, designed to provide eight high precision position measurements per track. The SCT barrel consists of four layers with 2112 detector modules in total. The modules themselves are made of 768 active strips in each of the two silicon layers. The two layers form an angle of 40 mrad to provide space points with minimal ambiguity. The barrel is complemented by two endcaps. Each endcap consists of 9 disks with 988 modules in total. Even though the shape and orientation of the endcap modules differs from the barrel modules, as shown in Figure 2, they contain the same number of strips. The SCT uses a binary readout system, meaning it only registers a hit if the amplified output voltage for a certain strip was above a preset discriminator threshold. This demands a sophisticated calibration of the threshold, since the performance requirements of the SCT include a hit efficiency greater than 99% and at the same time a noise occupancy smaller than $5 \cdot 10^{-4}$.

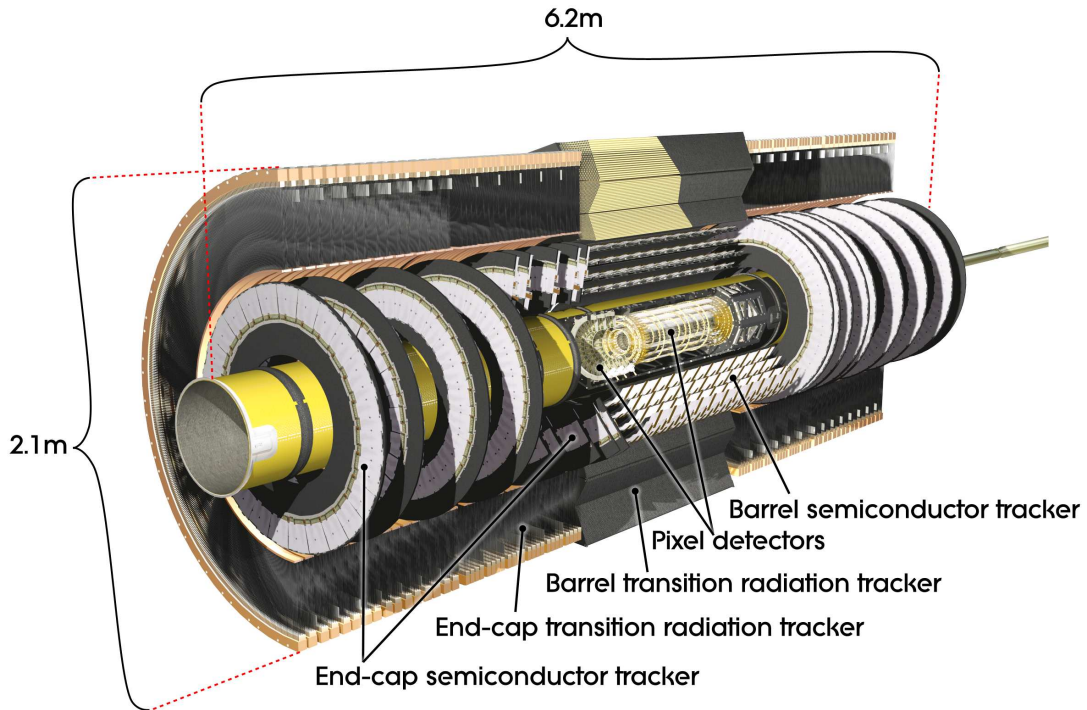
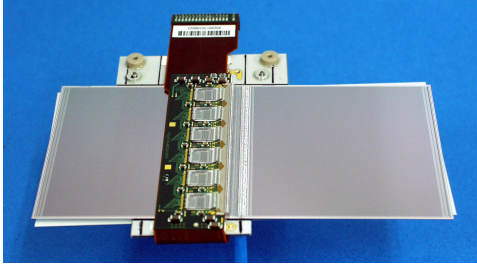
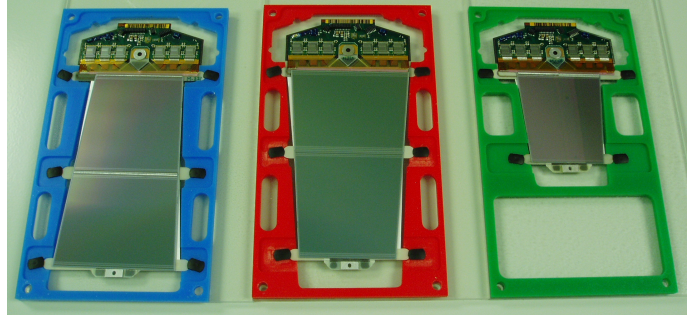


Figure 1: A cut-away view of the ATLAS Inner Detector, originally found in [1].



(a) Barrel modules



(b) Endcap Modules

Figure 2: The SCT barrel and endcap modules. There is one barrel module type and four endcap module types, three of them can be seen in b). The 40 mrad angle between the layers can be seen here.

The noise sources in semiconductor detectors are different kinds of leakage currents, like surface currents, reverse leakage current and current from thermal ionization. Finding a threshold value which fulfills this requirement gets more difficult over time, because the leakage current increases due to radiation damage. Fortunately, the time evolution of the leakage current can be predicted accurately using various models which consider the proton fluence and the operating temperature. More on this topic and on the SCT performance can be found in [1].

In this report, the time evolution of the SCT conditions data is analyzed. The main goal is to find correlations between different variables and relations between different parts of the detector. Those results will be used to test if the degradation of the detector is due to radiation damage and to check the origin of the mentioned radiation. Later, the behavior of individual modules which show a strange evolution of the conditions data is analyzed. One focal point is to identify strips which turned bad due to runaway effect: increasing leakage current increases the temperature, which in return reduces the resistance and thus increases the leakage current again. The presentation of results and the analysis is preceded by an brief explanation of the SCT calibration, the conditions data used, and the effect of radiation damage on the conditions data. The presentation of results and the succeeding analysis are divided in two parts: one focuses on the long-term performance of the detector and the other on indications for radiation damage. In the conclusion of the report we mention which investigations could be made in the future, since the findings of this report establish also new questions which couldn't be answered in the scope of this project.

2 SCT calibration and conditions data

2.1 Calibration between LHC fills

To ensure the fulfilling of the performance requirements, the threshold for every module has to be recalibrated [2] regularly between LHC fills. Among the recorded data during those calibrations are the module temperature, the leakage current, the equivalent noise charge (ENC), the gain and the threshold itself. For the later analysis, it is important to understand the ENC and especially how it differs from the noise occupancy. For ENC measurements, a charge of the order of magnitude of 1 fC is injected into the module front-end, followed by a scan of the module occupancy for different thresholds. The occupancy is 50 % at the threshold voltage corresponding to median of the input charge, which should be dominated by the injected charge, thus the gain can be calculated with this simple formula:

$$\text{gain [mV/fC]} = \frac{\text{threshold [mV] where occupancy is 0.5}}{\text{injected charge [fC]}}. \quad (1)$$

The 1σ region corresponds to the noise which added up to the injected charge, so the ENC can be obtained by dividing σ by the gain, which has the correct dimension of a charge. In other words, the ENC is a measure of the expected value of the noise. Occasionally, this threshold scan is conducted with no injected charge, measuring the noise occupancy instead. As it will be explained later in more detail, the noise occupancy is a measure for the tail of the noise and the ENC is then extrapolated assuming a Gaussian noise.

2.2 Prompt calibration loop

To ensure good data quality it is important to monitor the state of the detector during runs. For this reason, a subset of the events is reconstructed parallel to the data taking to obtain detector conditions data or even perform online calibration. For the SCT, no calibrations are performed during the this prompt calibration loop [4], but a special data stream triggered on empty bunch crossings (no collisions) is used to identify noisy strips. A noisy strip is a strip with an occupancy of more than 1.5 % of the time, which is an indication that this channel is not reliable. It is therefore excluded from the later reconstruction of the bulk of the events. Those are however not the only strips excluded from event reconstruction: strips or modules which appeared to be dead in the offline calibrations and the calibration loop are also not considered. The full set of reconstructed events is later used to obtain other conditions data, which are mentioned in the following.

2.3 Conditions data used in this work

This analysis focuses on three different kinds of conditions data: the number of noisy strips already defined in the previous section, the noise occupancy and the efficiency. The data used in this study does not come from the calibration between fills, but from the physics runs. The efficiency is obtained by relating the number of hit clusters in a module belonging to a reconstructed track to the number of missing clusters, called holes. A hole is present if a cluster is expected according to reconstructed tracks, but no corresponding hits were registered. The efficiency can be calculated as follows:

$$\varepsilon = \frac{N_{\text{clusters}}}{N_{\text{clusters}} + N_{\text{holes}}}. \quad (2)$$

For better visualization in logarithmic plots, the inefficiency $1 - \varepsilon$ is often used in the following. The noise occupancy is the detector occupancy due to noise. The occupancy can be defined as the mean number of hits above threshold per channel per event. A module occupancy of 1 would therefore mean that every channel registered a hit at every event. Because only noise above the discriminant threshold is registered and the expected value of the noise is way beyond the threshold, the noise occupancy is a measure for the tail of the noise.

The information about noisy strips is available at the level of individual noisy strips. The noise occupancy is given as the module average. The efficiency however is also averaged over the azimuthal angle φ ¹. Additionally, the barrel efficiency is averaged over z . In other words, the barrel efficiency for each run is only known as the layer average ².

¹In this work, cylindrical coordinates are used. The z -axis follows the beam direction. The endcap at positive z -direction is called endcap A, the other one endcap C.

²The layers are not labeled with numbers from 1 to 4, but from 3 to 6, where layer 3 is the inner layer.

2.4 Radiation damage and conditions data

To investigate the characteristics of the SCT radiation damage using conditions data, one first has to think about what specific features are expected to be seen in the data. This consideration starts with assumptions on the radiation: the radiation consists of particles created in the collisions, thus originating from the IP.. Because calorimeters are designed to interact with the particles, part of the radiation is made up of particles backscattered by the electromagnetic calorimeter. The radiation damages the sensors mainly by displacing silicon atoms from their crystal lattice. This causes the formation of new energy levels in the band gap and also a change of the effective charge carrier density. Going into more detail on why this ultimately results in an increase of leakage current would stretch the scope of this report too far, but it can be found in [5]. The second main damaging mechanism is the creation of electron-hole pairs in SiO₂ layers. While the electrons immediately travel to the next anode, the holes move much slower and get on the interface, acting as space charges disturbing the electronics.

If noise is increased by radiation damage, one would expect the noise occupancy to behave in a particular way.

1. It should be distance dependent, because the radiation intensity is proportional to r^{-2} when backscattering is neglected.
2. High radiation in one part of the detector would imply high radiation in another part, because the origin is the same. An other guess is therefore that the noise in different parts of the detector should be correlated.
3. The displacement damages recovers over time, because the displaced silicon atoms have a chance of recombination due to thermal movement, expected to be visible as a significant decrease in noise after LHC maintenance breaks.

3 Results and analysis

3.1 Time evolution of the number of noisy strips

The time evolution of the total number and fraction of noisy strips is shown in Figure 3. The number of noisy strips fluctuates in a dynamic range of about two orders of magnitude. In [1], this has also been noticed. It is mentioned that this is mainly due to so called single-upset events. It means that bits in the module electronics are flipped, changing for example the discriminator threshold of multiple strips at once if they share the same threshold register. If the threshold was lowered, all the affected strips become noisy. It is also stated that especially the endcap modules contribute to this large fluctuation. This investigation tried to replicate this insight. However, the σ of the distribution of the number of noisy strips only for barrel modules was not smaller than the σ when all modules were considered. Apart from the fluctuation, the number of identified noisy strips increases in the first months of the 2011 (7 TeV) runs. It then converges and rises up to a new limit during the 8 TeV runs. This is because luminosity increased, causing more single-event upsets. A recovery during downtime can not be observed.

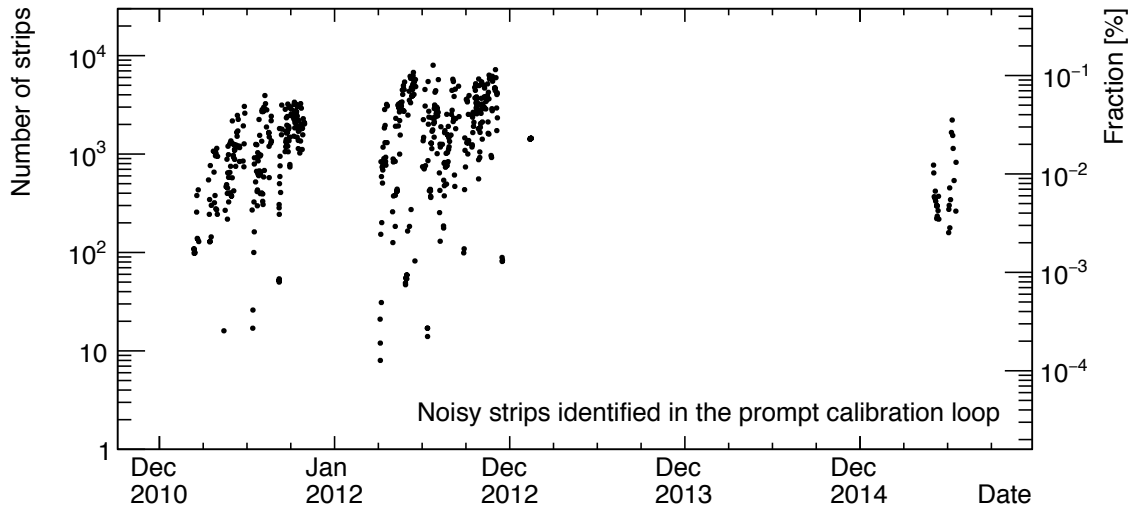


Figure 3: The number of noisy strips identified in the prompt calibration loop for each run for which this information has been uploaded, except for cosmic runs. Besides the raw noisy strip count, the relative number of noisy strips in the detector is indicated.

3.2 Time evolution of the noise occupancy

To get an idea of the noise occupancy of the detector, a histogram can be filled with all noise occupancy measurements for all modules. In 4, this has been done for all years of operation. Values for barrel and endcaps are shown separately. It can be observed that noise increased from 2011 to 2012, hinting the detector degradation. The σ of the 2012 noise occupancy is smaller, because the total runtime of the LHC in this year was longer. This allowed the SCT noise occupancy to reach stable values, as can be seen in Figure 5. The noise occupancy in the 2015 runs seems to be generally lower. This can be explained with the recombination of displacement damage. The LHC operation has only just started, so the noise occupancy is still expected to rise again, eventually exceeding the values of the previous years. The time development of the barrel noise occupancy in Figure 5 is also showing this recovery for the uptime in 2012.

The histograms raise two further questions. One of them is the small peak around a logarithmic noise occupancy of -3.3, with almost no counts at higher values. One of the performance requirements was that the noise occupancy is below this value, so the reason for this could be that the threshold is calibrated in such a way that this value is almost never exceeded, sacrificing efficiency in return. The fat tail with an additional peak of the endcap noise occupancy for 2015 is also noteworthy. This agrees with the high inefficiency observed in Figure 6b for 2015, since inefficiency and noise occupancy cannot be low at the same time. A further investigation of this is not in the scope of this project.

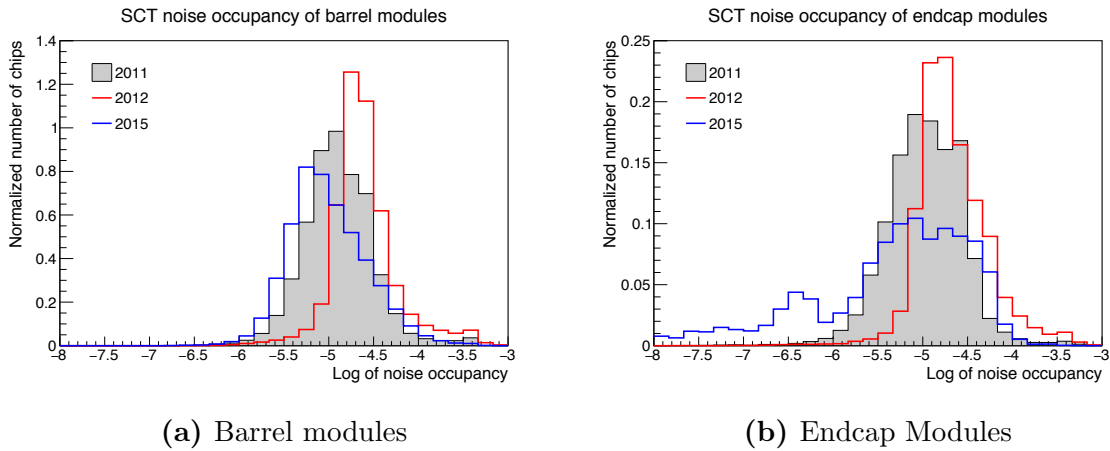


Figure 4: Visualization of how the distribution of the module average noise occupancy for the barrel (a) and for the endcaps (b) is changing over long timescales. The logarithm to base 10 is used and the statistical error is negligible because of the large amount of modules and runs. The years correspond to the 7, 8 and 13 TeV proton-proton runs, with data from cosmic runs being excluded.

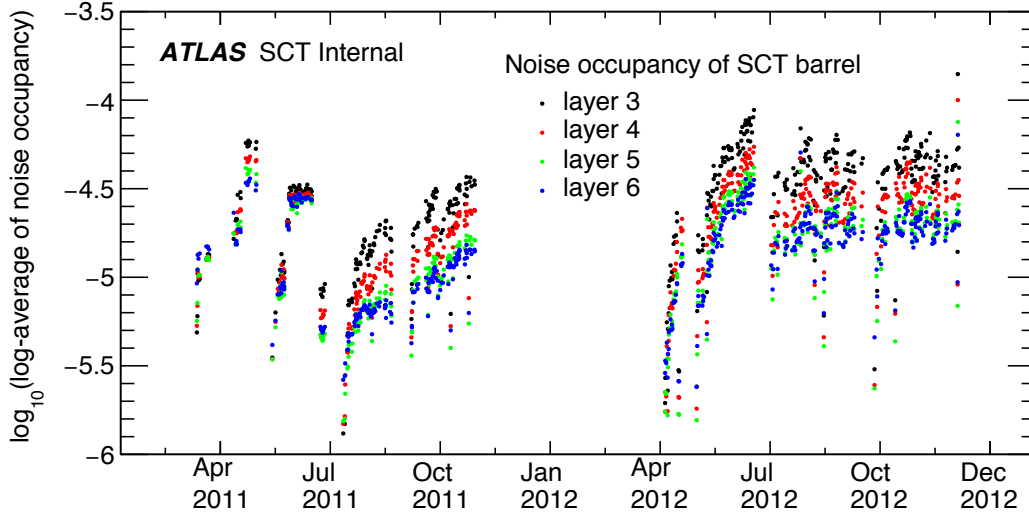


Figure 5: Time evolution of the noise occupancy for the different barrel layers. Note that the average of the logarithms was used, and not the logarithm of the average. This was done every time when noise occupancy had to be averaged, because of the large dynamic range of those values.

3.3 Time evolution of the efficiency

The efficiency seems to be more stable over time, as can be seen in Figure 7. It only appears to be slightly affected by maintenance breaks, also observable in 6: the 2015 inefficiency average also seems to be lower than in the previous years for now. An explanation could be provided by the different damage mechanisms. To keep the efficiency high, the electrical fields in the depletion zone need to be maintained. They are primarily disturbed by the space charges in the SiO_2 layers, and not by the displacement damage, which is mainly responsible for increasing noise. If displacement damage and space charges recover at different rates, the different recovery behavior of noise occupancy and efficiency could be explained with it. The 2012 data shows a peak at an inefficiency of 1. This data is all originating from a time period around June 2012, indicating a problem with the detector which is probably not originating from radiation damage.

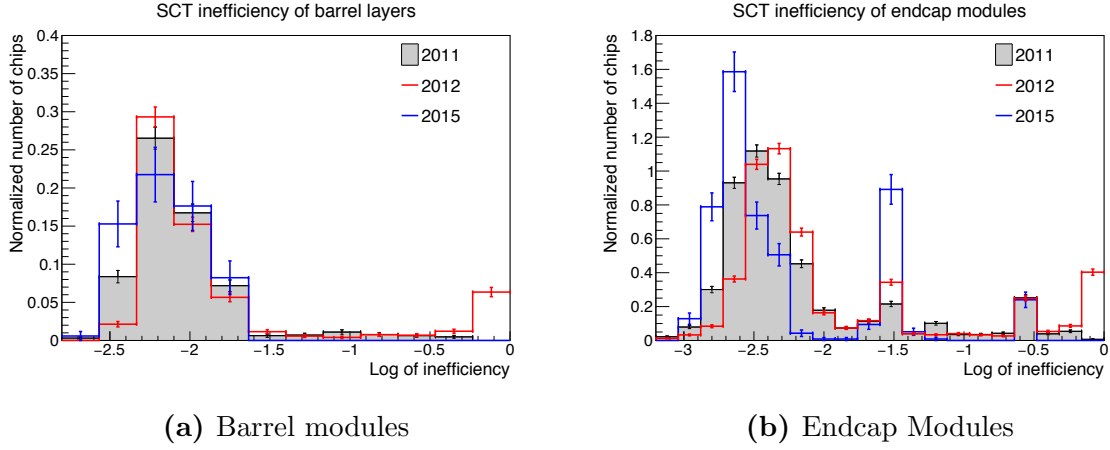


Figure 6: Time evolution of the inefficiency distribution. Note that this histogram is not filled with the inefficiencies of the individual modules. Instead, the endcap inefficiency is averaged over φ . This drastically reduces sample size, so the statistical errors are not negligible. The inefficiency for the barrel was additionally averaged over z , further reducing sample size.

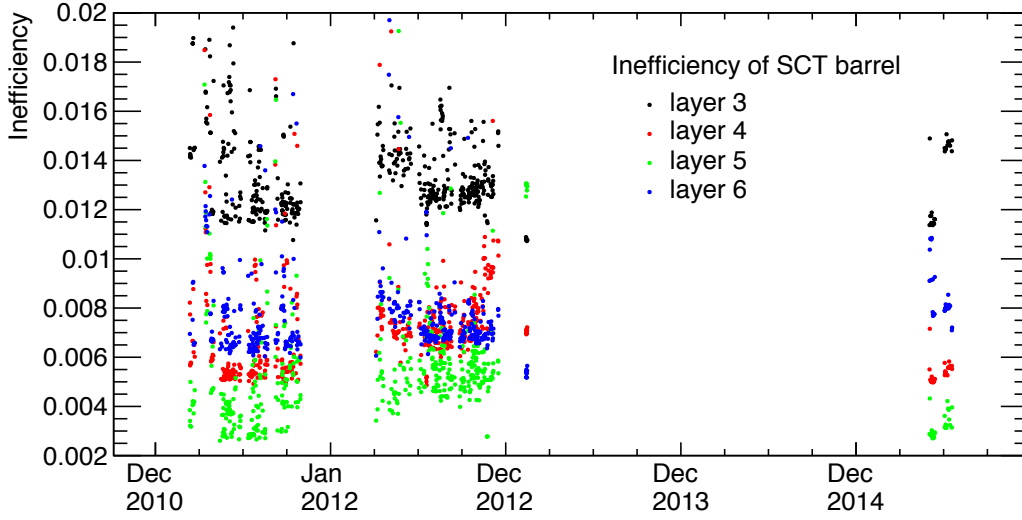


Figure 7: Time evolution of the barrel efficiency for all layers individually. The limits of the y-axis cut off the inefficiency at 0.02, the performance requirement, thus hiding the data points above it hinted by the histogram.

3.4 Correlation and distance dependence of the noise occupancy

To learn about the correlation of noise occupancy in different parts of the detector, it makes sense to plot the noise occupancy of one part against another part. The different barrel layers are chosen for this; the result is shown in Figure 8. For maximum correlation, the data points should be along a straight line. This seems to be the case, and it is a strong indication for radiation being a main reason for increasing noise. The data points which seem to be off in the region above a logarithmic noise occupancy -5.4 can be identified as the runs directly after long breaks, in particular the 13 TeV runs. They can thus be explained with the displacement recovery mentioned before. For lower noise occupancy, the linear trend doesn't persist. The intrinsic noise of the detector is probably dominating the radiation induced noise at those magnitudes. The linear correlations also allow us to test the assumptions on distance dependence. If we assume that noise is proportional to radiation intensity, which is itself proportional to r^{-2} , the ratio of the average noise occupancies of different layers (i, j) can be related to the average distance from the modules to the IP³:

$$\frac{\langle \text{NO}_i \rangle}{\langle \text{NO}_j \rangle} = \frac{\langle d_j^2 \rangle}{\langle d_i^2 \rangle}. \quad (3)$$

This formula yields the theoretical predictions in Figure 8, which the data is agreeing with, at least for layer 4. Layer 5 has a higher noise occupancy than expected, which could be explained by the presence of albedo particles. Comparing layer 6 with the others is more difficult. Noise in this layer is higher in general, because of the higher operational temperature (10 °C instead of 2.5 °C). The reason for this is the proximity to the TRT, which requires a higher operational temperature than the SCT. This can be taken into account using noise occupancy measurements from calibration runs after maintenance breaks, found in [1]. The combined result of the 2010 and 2012 calibrations is a factor of 1.7 with a statistical error of 2%. The noise occupancy of layer 6 in Figure 8 is divided by this factor. However, this seems to be a small overcorrection, especially when considering that the noise occupancy should generally lie above the theoretical guess because of the albedo particles.

³Because the actual distances from the modules to the IP need to be considered, one can not simply take the layer radius as the distance. Instead, the average module distance is $\langle d_i \rangle = \frac{R_i}{2} + \frac{r_i^2}{4a} \log \left(\frac{R_i - a}{R_i + a} \right)$, with $R^2 = a^2 + r_i^2$, the layer radius r_i and the barrel length $2a$.

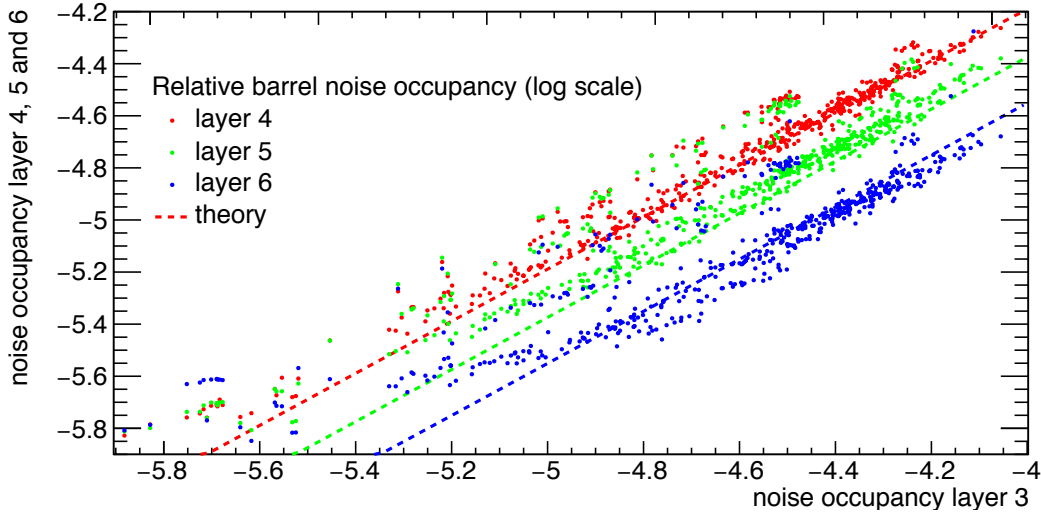


Figure 8: The log-average noise occupancies of the three outer barrel layers versus the noise occupancy of the innermost layer. A point corresponds to a single non-cosmic run with conditions data available. The noise occupancy of layer 6 was scaled with a factor of 0.59 to account for differences in operational temperature.

3.5 Analyzing individual modules

The relative noise occupancy of one module over time is shown in 9. Although fluctuating around the average, it undergoes sudden jumps to higher noise occupancies, followed by slower decreases. A first guess would be that the jumps are due to displacement damage done by an incident particle which then slowly recombine over time. In [5], it is explained that displacement damage doesn't affect one atom at the time, but the displaced atoms displace around 1000 other atoms immediately. They still recombine one at a time. This could explain the sudden jumps and slow decreases. However, the fact that some jumps are also happening in the other direction challenge this explanation. Also, the sudden increases sometimes jump up several orders of magnitude; a close-up on one of this events can be seen in Figure 10. Those events are difficult to interpret, because parameters like starting point, end point and decay rate are never the same. The decay rate can fluctuate between 1 and 10 days. To check if those events are due to the runaway effect mentioned at the beginning, which should happen at currents above 5 mA, data obtained from calibration runs was visualized in Figure 11. No outstanding behavior of the temperature or the current can be observed at the time where the event in 10 happened. It is unclear if this really is the case, or if calibration runs are just not frequent enough to sample the anomaly in temperature and current. It is also noteworthy that the ENC was not increasing as dramatically as the noise occupancy was. At least, this gives us a hint on how the noises probability density function was changing during the sudden-increase-events: the expected value seems to be unchanged and the probability of large noise charges above the threshold was increasing.

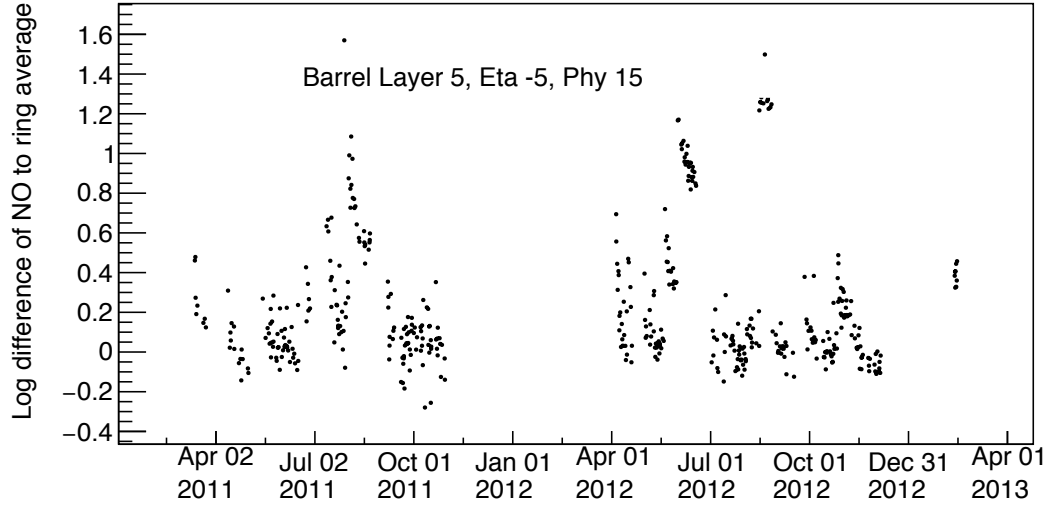


Figure 9: The noise occupancy of one barrel module divided by the log-average noise occupancy of all the modules at the same position, except for a different angle φ . If one would instead plot the absolute noise occupancy of this one module, the sudden increases would be less prominent, but one would also see a slight general increase in noise occupancy, apart from the sudden increases.

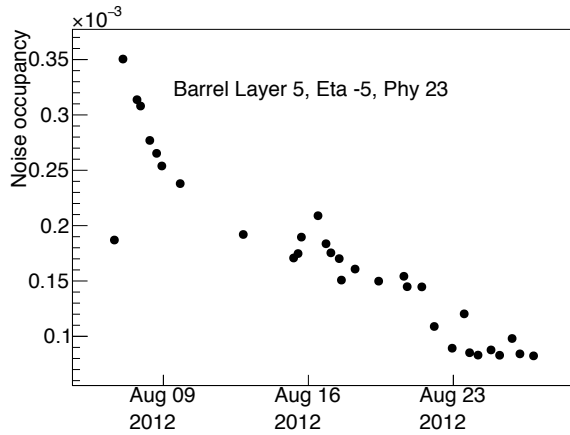


Figure 10: A close up on one of the sudden increases in noise occupancy as shown in 9, this time for an other module in the same layer. Also, the absolute noise occupancy is shown instead of the relative. The noise occupancy before and after the shown time period was stable around 10^{-5} .

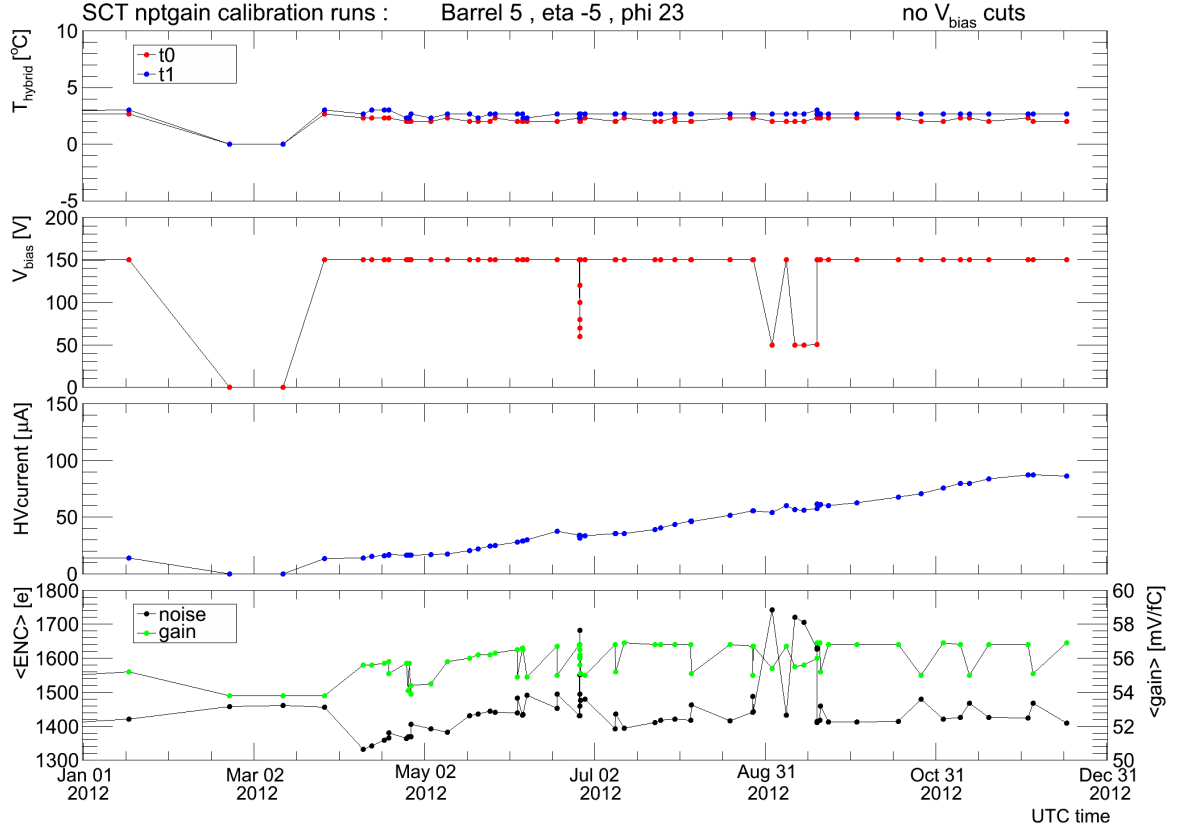


Figure 11: Other calibration data for the same module as shown in 10, including the operational temperature, the current and the equivalent noise charge.

4 Conclusion

Even in a high-radiation environment like the surroundings of the LHC interaction points, the SCT performs stably, although radiation damage yields a slow degradation over time. This could be seen in the long-term evolution of the noise occupancy, which shows features expected from a degradation due to radiation damage: distance dependence, correlation between different parts of the detector and recovery. It indicates that the radiation is mainly coming from the interaction point. Still, it converges to a constant value during long times of operation. It would be interesting to see to what value it converges in the current runs with 13 TeV. It is expected to be a higher value due to higher luminosity.

The noise occupancy of individual modules behaves in a less stable way. The reason for sudden, irregular increases could not be found. Perhaps it could be found if the exact particles with their energies involved in the damaging process are known, and the temperature and current are sampled in a much higher rate. As every module shows this behavior, it would only be necessary to monitor a few modules with the higher sample rate to get more information. Knowing all tracks hitting the module is more challenging. Most tracks belong to events which are unusable for physics and get triggered away, but if all events with tracks through the monitored modules would be kept, this could be achieved.

References

- [1] ATLAS Collaboration, *Operation and performance of the ATLAS semiconductor tracker*, JINST **9** (2014) P08009 [arXiv:1404.7473 [hep-ex]].
- [2] ATLAS Collaboration, *The Data acquisition and calibration system for the ATLAS semiconductor tracker*, JINST **3** (2008) P01003.
- [3] ATLAS Collaboration, *The ATLAS Experiment at the CERN Large Hadron Collider*, JINST **3** (2008) S08003.
- [4] ATLAS Collaboration, *Prompt data reconstruction at the ATLAS experiment*, J. Phys. Conf. Ser. **396** (2012) 022049.
- [5] H. Spieler, *Semiconductor Detector Systems*, OUP Oxford (2005).